UC Berkeley

UC Berkeley Previously Published Works

Title

Structure and Dynamics of Polysulfide Clusters in a Nonaqueous Solvent Mixture of 1,3-Dioxolane and 1,2-Dimethoxyethane

Permalink

https://escholarship.org/uc/item/9641d5db

Journal

Chemistry of Materials, 31(7)

ISSN

0897-4756

Authors

Andersen, Amity
Rajput, Nav Nidhi
Han, Kee Sung
et al.

Publication Date

2019-04-09

DOI

10.1021/acs.chemmater.8b03944

Peer reviewed

eScholarship.org Powered by the California Digital Library
University of California

Structure and Dynamics of Polysulfide Clusters in a Nonaqueous Solvent Mixture of 1,3-dioxolane and 1,2-dimethoxyethane

Amity Andersen,[1*] Nav Nidhi Rajput,[2,4†] Kee Sung Han,[1,4] Huilin Pan, [1,4] Niranjan Govind,[1] Kristin A. Persson,[2,3,4] Karl T. Mueller,[1,4] Vijayakumar Murugesan[1,4*]

[1]Pacific Northwest National Laboratory, Richland, Washington 99352, United States

[2]Lawrence Berkeley National Laboratory, Berkeley, California 94720, United States

[3]Department of Materials Science and Engineering, University of California, Berkeley, California 94720, United States

[4]Joint Center for Energy Storage Research (JCESR), Lemont, Illinois 60439, United States

ABSTRACT: Molecular clustering and associated dynamic processes of lithium polysulfide species were unraveled using classical molecular dynamics and *ab initio* metadynamics calculations. The spectroscopic signatures of polysulfide clusters were analyzed using a multimodal analysis including experimental and computational NMR and XAS spectroscopies. Lithium polysulfide solutes (Li_2S_4, Li_2S_6, and Li_2S_8) and their mixtures in 1,3-dioxolane and 1,2-dimethoxyethane (DOL/DME) solvent undergo aggregation driven by intramolecular Li-S interactions, leading to distributions of cluster sizes which could critically influence the functioning of lithium-sulfur batteries. Representative polysulfide clusters with systematic increases in molecular size were extracted from the classical MD trajectories for subsequent structural and spectroscopic property calculations using DFT analysis. Structural analysis of these clusters reveal progressively decreasing solvent involvement in Li^+ coordination varying from Li_2S_4 to Li_2S_8, with more pronounced variation and changes in DME compared with that of DOL. These observations are reflected in the analysis of the experimental and theoretical ^7Li and ^{17}O NMR chemical shifts and PFG-NMR diffusion measurements. A comparison of experimental and theoretical S K-edge XANES spectra show that relatively large lithium sulfide chain clusters are likely to occur in the DOL/DME-solvated lithium sulfide systems. *Ab initio* metadynamics simulations and NMR analysis indicates that Li^+ solvated by only the solvent can occur through Li^+ dissociation from sulfide chains. However, the occurrence of "sulfide-free" Li^+ is a minor mechanism compared with the dynamic aggregation and shuttling processes of polysulfide solvates in DOL/DME based electrolytes of Li-S battery. Overall, atomistic insights gained about clustering and lithium exchange dynamics will be critical for predictive understanding of polysulfide shuttling and nucleation process that dictates the Li-S battery performance.

1. INTRODUCTION

The lithium-sulfur (Li-S) battery is a promising candidate for higher gravimetric energy storage due to its favorable theoretical specific energy density (2600 Wh/kg), specific capacity (1675 mAh/g), low expensive compared to other state-of-the-art lithium-ion batteries, and the natural abundance and environmentally-benign property of elemental sulfur.[1-4] In practice, however, Li-S batteries have several issues that need to be addressed including the formation of soluble and insoluble species during cycling and the electrical insulating properties of elemental sulfur and lithium sulfide (Li_2S). In particular, the formation of highly soluble polysulfide intermediates in the electrolyte during discharging/charging cause active material loss and leads to rapidly diminishing capacity through a mechanism where the polysulfide species act as redox "shuttles" between the cathode and anode and can participate in parasitic reactions with the Li metal anode leading to dendritic growth.[3, 5-7]

Strategies have been explored to protect the anode using confinement or protective layers.[1, 5] Thus far, these anode-centric strategies fail to block polysulfide species and restrict the volumetric energy density. Another, less-explored approach is to suppress the dissolution of polysulfide species and improve electrochemical stability through electrolyte design optimization. Due to their low cost and high propensity to dissociate and solvate salts because of relatively strong Lewis basicity from oxygen lone pairs,[8, 9] glymes ($CH_3(-OCH_2CH_2-)_nOCH_3$) are promising solvents in the electrolytes for lithium-sulfur

batteries. In particular, 1,2-dimethoxyethane (DME) together in a binary solvent mixture with 1,3-dioxolane (DOL) and with 1 M lithium bis(trifuoromethanesulfonyl)imide (Li-TFSI) is one of the most favorable and widely-used electrolytes for lithium-sulfide cells.[1, 6] The DOL/DME solvent system, however, suffers from the obstacle that polysulfides are significantly soluble and thus facilitate the shuttle process and subsequent parasitic reactions.[1] Therefore, there is a need to improve the electrolyte design to lower the solubility of dissolved polysulfides, increase the chemical stability and enhance the ionic conductivity.

A number of experimental and theoretical studies have been performed to shed light on the dissolution process and chemical stability of polysulfides.[10-26] For example, recent works on polysulfide disproportionation reactions leading to sulfide radicals (mainly S_3^{-*}) have been observed in both experiment and theory. However, considering relatively low energy barrier of disproportionation reactions, these radicals can recombine with parent polysulfide species and possibly exhibit in a dynamic equilibrium within electrolyte solution.[10,27] Over the longer time regime of the Li-S electrochemical process, polysulfide aggregation and lithium exchange processes are critical for enhancing the performance of Li-S battery. Hence, the key knowledge gap remains regarding the exact molecular structure and transport mechanisms of lithium polysulfide species. For example, do polysulfide anions diffuse across the battery as anion species or as neutral lithiated species?[14] Are lithium ions strongly bound to the solvated polysulfides, or can the lithium ions detach from the polysulfides and diffuse into electrolyte? Do multiple polysulfide species aggregate in electrolyte solution?

The aim of this study is to delve into these open questions about the structure and dynamics of the soluble polysulfide species in the DOL/DME electrolyte system and gain deeper insight into these complex molecular systems. With a fundamental understanding of the nature and processes of the solvated polysulfide intermediates in the nonaqueous electrolyte, further strategies can be devised to improve the performance and longevity of lithium-sulfur batteries such as tailoring the electrolyte properties through novel formulations (e.g., new electrolyte components, mixtures, additives).

2. EXPERIMENTAL METHODS

2.1 Samples Preparation

Nominal 1 M Li_2S_n dissolved in DOL/DME (n = 4, 6, and 8) solutions were obtained by mixing stoichiometric Li_2S and S_8 in DOL/DME (1:1, v:v) solvent, and stirring at 60 °C in oil bath for 1-10 hours in the Ar-filled glove box. This dissolution and reaction based sample preparation may result in distribution of various Li_2S_x species. However based on our previous mass spectrometry studies, solution based synthesis tends to provide the targeted polysulfide species (such as Li_2S_4, Li_2S_6 or Li_2S_8) as a major constituent. Hence, it is assumed that targeted chemical composition represents the prepared solution.

2.2 Nuclear Magnetic Resonance (NMR) and Pulsed Field Gradient (PFG) NMR measurements.

^{17}O NMR and diffusion measurements were performed on a 600 MHz NMR spectrometer (Agilent, USA) with a 5 mm z-gradient liquid probe (Doty Scientific, USA), which has a maximum gradient strength of ~31 T/m. ^{7}Li NMR spectra were obtained on a 750 MHz NMR spectrometer (Agilent, USA) with HX probe. The ^{7}Li and ^{17}O chemical shifts of 0 ppm for a 1 M $LiCl/H_2O$ solution and dilute water were used as external references, respectively. Diffusion coefficients of lithium polysulfides (i.e. Li^+ cations) and solvent molecules (DOL and DME) were measured using ^{7}Li and ^{1}H pulsed field gradient (PFG) NMR, respectively, using vender supplied 13-interval bipolar gradient PFG sequence (Dbppste, vnmrj 4.0, Agilent, USA) over the temperature range of 20 ~ 50 °C. The echo heights, $S(g)$, recorded as a function of gradient strength, g, were fitted with the Stejskal-Tanner equation, $S(g) = S(0)exp[-D(\gamma g\delta)^2(\Delta-\delta/3)]$, where $S(g)$ and $S(0)$ are the echo heights at the gradient strengths of g and 0, respectively, D is the diffusion coefficient, γ is the gyromagnetic ratio of ^{7}Li or ^{1}H, Δ is the time interval between the two pairs of bipolar gradient pulses (also called the diffusion time), and δ is the time of a pair of gradient pulses applying. The gradient strength was varied over 15 equal steps and the maximum gradient strength was chosen accordingly to get a proper decay of the echo profile in each measurement. The 90° pulse and two delays, Δ and δ were chosen properly for each PFG-NMR and fixed in all measured temperatures. We estimated an effective hydrodynamic radius (r^*) for Li^+ cations (r_{Li}^*) and DME molecules (r_{DME}^*) using the Stoke-Einstein equation of diffusion based on the assumption that most Li^+ cation dissolved by the DME molecules then the effective hydrodynamic radius of DOL is similar to its molecular size ($r_{DOL}^* \approx r_{DOL}$).[6, 12, 13]

2.3 X-ray spectroscopy.

Sulfur K-edge x-ray absorption near-edge spectroscopy (XANES) measurements were performed at the Canadian Light Source (CLS) beam-line port SXRMB. Monochromatic X-rays with an energy resolution of about 0.25 eV and photon flux of 1×10^{11} photons/seconds are generated using a Si(111) double-crystal monochromator. The beam is subsequently focused using a set of Toroidal mirrors, with the spot size of 1×8 mm^2. All spectra were collected under fluorescence mode. Droplets of polysulfide solutions were packed in kapton films and measured at different sample volume and regimes to ensure optimal sample thickness and uniformity. In detail, 5 – 10 µl of polysulfide solution is sandwiched between ~2×2 cm^2 kapton films and subsequently sealed with kapton tap and mounted onto sample holder with multiple slits and mechanical sample positioning system. All sample packaging were performed inside the nitrogen filled glove

box to avoid parasitic reactions with oxygen/humidity. The position of white line of elemental sulfur (S_8) plotted in derivative mode is used as energy reference point (2470.5eV) for all the spectra (see SI). An energy range of −20 eV to +50 eV with respect to this reference position with step size of 0.2 eV was used for the collection of the XANES data. The ATHENA package was used for the background reduction and also for self-absorption correction using absorption energy mode with chemical composition of the solution (Figure S7).

3. THEORETICAL METHODS

3.1 Classical molecular dynamics simulations.

Classical molecular dynamics (MD) was performed using the GROMACS MD simulation package version 5.1.2.[28] The initial configurations were obtained by randomly packing molecules in a periodic cubic box of size 60×60×60 Å^3 using PACKMOL.[29] The initial configuration was first minimized using the steepest descent method, employing a convergence criterion of 1000 kcal/mol·Å and then using the conjugate-gradient energy minimization scheme employing a convergence criterion of 10 kcal/mol·Å. The systems were equilibrated in the isothermal-isobaric ensemble (constant NPT) using the Berendsen barostat to maintain the pressure of 1 bar with a time constant of 2 ps for 2 ns.[30-32] All systems were then melted at 400 K for 2 ns and subsequently annealed from 400 to 298 K in three steps for 3 ns. Finally, production runs of 20 ns were then obtained in the canonical ensemble (NVT) using an improved velocity-rescaling algorithm proposed by Bussi et. al.[31] with a time constant of 0.1 ps at 298 K. The simulation time was long enough to adequately sample the Fickian (diffusive) regime of all systems and the results were averaged over at least two independent realizations of the same system. All other simulation details and force field parameters are the same as those in our previous published work.[13]

3.2 NMR chemical shift calculations.

Li_xS_y solvated cluster systems, ranging in sizes from 152-377 atoms, were extracted from the snapshot frames of the classical molecular dynamics simulation trajectories using the VMD software.[33] Magnetic shielding calculations for the Li_xS_y solvated cluster systems were performed using the NWChem quantum chemistry software.[34] The PBE0 density functional[35, 36] were used for all Li_xS_y solvated cluster calculations along with the 6-31G* Gaussian basis set.[37, 38] van der Waals interactions were treated using the Grimme dispersion correction (D2).[39] Magnetic response calculations to calculate ^{7}Li and ^{17}O magnetic shieldings used the gauge-including atomic orbital (GIAO) linear-response density functional theory (DFT) implementation in NWChem. Prior to magnetic shielding calculations, geometry optimization was performed for each of the Li_xS_y solvated cluster structures. To lower the expense of the geometry optimization calculations, we used a Stuttgart large core effective core potential (ECP) and basis set for sulfur;[40] the sulfur Stuttgart ECP/basis set was replaced with the sulfur 6-31G* basis set in subsequent response calculations (magnetic shielding and XANES).

Chemical shifts were calculated from the calculated Li_xS_y solvated cluster magnetic shielding using $\delta_{cluster} = \sigma_{ref} - \sigma_{cluster}$ where σ_{ref} is the calculated magnetic shielding of a suitable reference compound for the nuclei of interest. We used an aqueous solvated Li^+ cluster model to calculate σ_{ref} for ^{7}Li and a dimethyl sulfoxide (DMSO) molecule to calculate σ_{ref} for ^{17}O.

The ^{7}Li reference Li^+-water cluster was constructed by first randomly solvating a single Li^+ cation located at the center of a 15×15×15 Å^3 box with 112 water molecules (for a density of 1 g/cm^3) using the PACKMOL program. The geometry of this system was optimized with the CP2K hybrid Gaussian/plane-wave basis set quantum chemistry software.[41, 42] Gaussian double-zeta valence-polarized (DZVP) MOLOPT basis sets[43] and Goedecker-Teter-Hutter (GTH) norm-conserving pseudopotentials[44-46] for core electrons were used in the CP2K calculations with an auxiliary plane-wave basis set having a 300 Ry energy cut off. The CP2K calculations utilized the nonlocal van der Waals density functional of Vydrov and Van Voorhis.[47-49] Following the optimization of the water-solvated Li^+ box, a NVT *ab initio* molecular dynamics (AIMD) simulation was ran using the optimized structure for 2.5 ps at 298.15 K with the canonical sampling through velocity-rescaling (CSVR) method of Bussi et al.[31] A subsequent NPT AIMD simulation was ran using the final NVT structure for 2.5 ps at 298.15 K and 1 atm using the methods of Bussi et al.[31, 32] The auxiliary plane-wave basis set energy cut off was increased to 600 Ry for the NPT AIMD simulation. The time step for the NVT and NPT simulations was 0.5 fs.

A Li^+-centered cluster with 55 water molecules surrounded the Li^+ cation (~7 Å water shell) was extracted from the final NPT AIMD periodic box snapshot using VMD. Further AIMD simulation using NWChem with the same basis sets, density functional, and Grimme dispersion correction as those used for the solvated Li_xS_y clusters was performed for 750 fs with a time step of 0.25 fs and at 298.15 K using the CVSR thermostat of Bussi et al. Solvation effects for the extended bulk water system on the Li^+-water cluster were included with the implicit solvation model of Klamt (i.e., COSMO).[50] The ^{7}Li magnetic shielding was calculated with NWChem on the final AIMD Li^+-water cluster snapshot.

The geometry optimization and ^{17}O magnetic shielding calculations of DMSO molecule were performed with the same basis sets and density functional used for the solvated Li_xS_y clusters. DMSO is a secondary ^{17}O reference, and the resulting chemical shifts from the calculated values were adjusted to the primary reference of liquid water by adding the neat DMSO's experimental chemical shift with respect

to the liquid water reference (+12 ppm[51]) to the calculated chemical shift with respect to DMSO.

3.3 XANES calculations.

X-ray absorption near edge structure (XANES) spectra were calculated using the restricted excitation window TDDFT (REW-TDDFT)[52-56] approach, including multipole contributions to the oscillator strengths, as implemented in NWChem using the same basis sets and exchange-correlation functional as in the NMR calculations described earlier. This approach, which involves defining a restricted subspace of single excitations from the relevant core orbitals and no restrictions on the target unoccupied states, is valid because excitations from the deep core states are well separated from pure valence-level excitations. We have successfully used this approach in several studies[57-62] over the last few years including studies on the K-edge spectra of sulfur in dissolved lithium polysulfide species in Li–S batteries.[10]

3.4 Ab Initio metadynamics simulations.

Similar to the ^{7}Li NMR Li^+-water reference system construction and simulation described in Section 3.2, single monomer Li_2S_4, Li_2S_6, and Li_2S_8 molecules placed at the center of 16×16×16 Å^3, 16×16×16 Å^3, and 17.5×17.5×17.5 Å^3 boxes, respectively. For the Li_2S_4 monomer system, a 50-50 mixture of 12 DME and 12 DOL molecules were calculated to occupy the remaining volume of the box based on their 0.8683 g/cm^3 (DME) and 1.06 g/cm^3 (DOL) liquid densities, respectively. Likewise, a 50-50 mixture of 12 DME and 12 DOL molecules and a 50-50 mixture of 15 DME and 15 DOL molecules were selected to occupy the remaining volumes in the Li_2S_6 and Li_2S_8 monomer systems, respectively. Each of the three Li_2S_y monomer systems were solvated with their respective DOL/DME mixtures using the PACKMOL program. The CP2K software was used to perform optimizations, NVT simulations, and NPT simulations in the same fashion as those performed for the ^{7}Li NMR Li^+-water reference system specified in Section 3.2 (i.e., same types of basis sets, pseudopotentials, NVT/NPT thermostat, NPT barostat, NVT/NPT temperature, and NPT pressure. Unlike the ^{7}Li NMR Li^+-water reference system simulation procedure of Section 3.2, the SHAKE algorithm[63] was used for hydrogen-bearing bonds (1.1 Å for C-H bonds) to extend the time step of the NVT and NPT simulations to 1 fs. The simulation time for all of the NVT and NPT DOL/DME-solvated Li_2S_y system simulations was 5 ps.

Following the NPT simulations, NVT metadynamics simulations were performed on each of the DOL/DME-solvated Li_2S_y monomer systems using the final NPT trajectory frame structures and cell lattice parameters. Each of the metadynamics simulations used two collective variables to scan 1) the monomer sulfur coordination number and 2) the DOL/DME solvent oxygen coordination number of the one of the two lithium atoms in each of the Li_2S_y monomer systems. A harmonic wall potential constraint of 1000 kcal/mol was placed on the Li-S distance of the other Li atom (with r_o=2.7 Å) to allow for the scanning of the free energy of a single Li migration to and from the sulfur chain monomer. Small repulsive Gaussian hills with a height of 2×10^{-3} Hartree and width of 0.2 Hartree were added at a frequency of every 50 time steps for both the Li-S and Li-O coordination number collective variables.

4. RESULTS AND DISCUSSION

4.1 Origin of Li_xS_y clustering phenomena.

Figures 1a-d show the MD simulations final snapshot structures of the DOL/DME-solvated 1 M of Li_2S_4, Li_2S_6, Li_2S_8, and Li_2S_4-Li_2S_6-Li_2S_8 mixture, respectively. From our MD simulations, Li_2S_y monomer units readily form dynamic clusters in the DOL/DME solvent under pure as well as mixture systems. From the Li^+-S, Li^+-O(of DME), Li^+-O(of DOL) pair distribution function (PDF) and number integrated pair distribution functions (NIPDF) shown in the supplemental information (see SI, Figure S1), it is evident that the Li-cation preferentially interact with DME than DOL molecules. Unlike the cyclic DOL molecule, the flexible hydrocarbon chains of the DME molecule can engage in bidentate formation which promotes interaction with Li^+. In addition, the Li^+-S association is greater than either the Li^+-O(DME) or Li^+-O(DOL) association, indicating that the Li^+-S is a more prevalent interaction than the solvent Li^+-O interactions. When comparing the Li_2S_4, Li_2S_6, and Li_2S_8 systems, the first-shell Li^+-S coordination number is greatest for the smaller sulfide, Li_2S_4, compared with the larger sulfides, Li_2S_6 and Li_2S_8, which are close in first-shell Li^+-S coordination number. On the other hand, the first-shell Li^+-O(DME) coordination number slightly increases with the sulfide monomer size from Li_2S_4 to Li_2S_8.

Figure 1e shows, the distribution of $(Li_2S_y)_z$ cluster sizes for the DOL/DME-solvated Li_2S_4, Li_2S_6, and Li_2S_8 systems averaged over the respective classical MD trajectories. The distribution represents the most persistent cluster sizes for each of the three Li_2S_y systems over time. The most prevalent cluster size of the Li_2S_4 system is $(Li_2S_4)_3$ followed by the monomer Li_2S_4. The Li_2S_6 and Li_2S_8 systems have sparser distributions of persistent cluster sizes with cluster sizes extending beyond the Li_2S_4 system maximum cluster size. The most prevalent cluster size for the Li_2S_6 system is $(Li_2S_6)_2$, and the frequency of the next most prevalent clusters sizes Li_2S_6, $(Li_2S_6)_4$, $(Li_2S_6)_7(LiS_6)^-$, $(Li_2S_6)_{16}$ are comparable. For the Li_2S_8 system, the most prevalent cluster sizes are $(Li_2S_8)_2$ and $(Li_2S_8)_{20}(LiS_8)^-$ with the latter cluster being larger than the maximum cluster size for the Li_2S_6 system. Unlike the Li_2S_4 system, persistent, fully DOL/DME solvent-solvated Li^+ are observed in the Li_2S_6 and Li_2S_8 system cluster size distributions with the frequency of DOL/DME-solvated Li^+ being higher in the Li_2S_8 system (see Figure 1e). The increased DOL/DME solvation of Li^+ with increasing sulfide monomer size agrees with the NIPDF trends discussed earlier.

We compared these cluster sizes with the effective hydrodynamic radius of Li^+ cations (r_{Li}^*) and DME molecules (r_{DME}^*), which tend to increase with decreasing sulfide monomer size (Figure 2). It is in reasonable agreement with the cluster sizes determined by the MD trajectories, if it considers the cluster sizes smaller than 60~80 number of atoms (Figure 1e). In general, it is hard to observe the (liquid) NMR signal from the larger clusters due to the colossal line broadening resulting from the diminished mobility.[12, 64] Therefore, the larger clusters like a $(Li_2S_6)_{16}$, $(Li_2S_8)_{10}$ and $(Li_2S_8)_{20}(LiS_3)^-$ may not affect the diffusion measurement by using PFG-NMR. It also shows that the r_{DME}^* is smaller (~3 times) than the r_{Li}^* due to the existence of a free DME molecules, which are not participating in the cluster formations. The gradual negative shift of ^{17}O NMR peak from -24 ppm of a free DME molecules with decreasing sulfur chain length (Figure 6) suggests that the interaction of

DME molecules with Li^+ cations becomes stronger with decreasing chain length. The gradual increase of the effective hydrodynamic radius of DME (r_{DME}^*) also suggests that the interaction of DME molecules with Li^+ cations becomes stronger with decreasing length of lithium polysulfide chains.

Figures 3a-f show the structures of DFT-optimized clusters extracted by from frames of the pure Li_2S_4 in DOL/DME classical MD trajectory (see Figure 1a). These close-up structure renderings demonstrate the sharing of lithium cations between two or more S_4^{2-} chains (Figures 3b-f and Table S1 listing atom coordination number and types of the Li atoms). In all six $(Li_2S_4)_z$ (z=1-6) cases, lithium cation joint coordination between the sulfur atoms of the sulfur chains and the solvent oxygen atoms occurs. Sulfur-only coordination with the lithium cations also occurs in clusters $(Li_2S_4)_z$ (z=2-4,6) (see Figures 3b-d,f and Table S1). With large DOL/DME-solvated $(Li_2S_4)_6$ cluster optimized with DFT, we observed few close Li-Li contacts which are shorter than the Li-Li distances in bcc bulk lithium metal (3.039 Å). At these distances, the nearest Li atoms share the same DME O atoms, creating four-fold coordinated DME O atoms (see Table S1). Looking at the next largest cluster, $(Li_2S_4)_5$, we see instances of Li atoms sharing the same DME O atoms, but no close Li-Li contacts. It is possible that, with greater amounts of aggregate sulfur, the Li^+ repulsive interactions are more effectively screened by the sulfur and solvent oxygen coordinations for the $(Li_2S_4)_z$ clusters. The pure Li_2S_4 MD trajectory shows the formation of clusters greater than six Li_2S_4 monomer units (as shown in Figure 1e), but the DFT optimization and subsequent response NMR and XANES calculations become very expensive for such larger clusters. However, the $(Li_2S_4)_z$ (z=1-6) results allow us to infer the trends in structural, NMR, and XANES features as cluster size increases. Figures 4a-d and 5a-c show the DFT-optimized clusters for the DOL/DME-solvated Li_2S_6 and Li_2S_8 clusters extracted from frames of the pure Li_2S_6 MD trajectory represented by Figure 1b and 1c, respectively. The $(Li_2S_6)_z$ (z=1-4) and $(Li_2S_8)_z$ (z=1-3) show similar lithium coordination features to that of the $(Li_2S_4)_z$ (z=1-6). $(Li_2S_4)_z$, $(Li_2S_6)_z$, and $(Li_2S_8)_z$ systems show joint sulfur chain and DOL/DME oxygen coordination at sulfur cluster-DOL/DME solvent interfaces. For the larger clusters $(Li_2S_6)_3$, $(Li_2S_8)_2$, and $(Li_2S_8)_3$, internal cluster sulfur-only lithium coordination is also found. However, the sharing of DME O atoms between adjacent Li^+ is rarer for the $(Li_2S_6)_z$ (z=1-6) clusters and nonexistent for the $(Li_2S_8)_z$ (z=1-3) clusters (see Tables

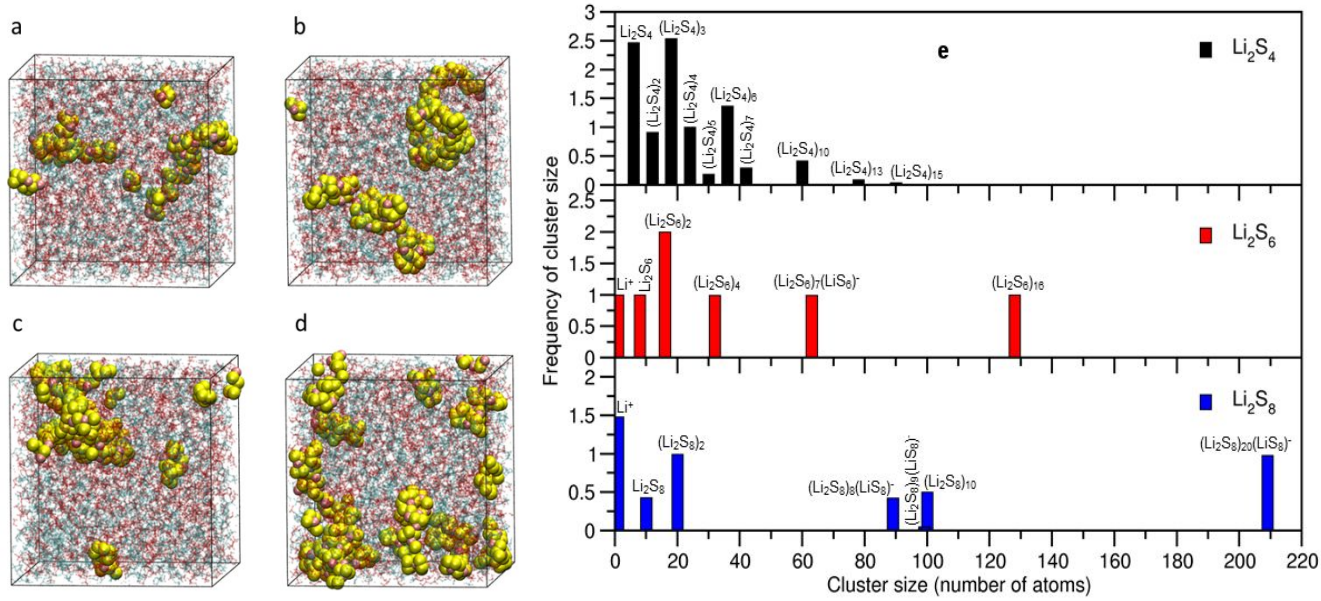

Figure 1. Final structures from classical MD simulations for a) Li_2S_4, b) Li_2S_6, c) Li_2S_8, and d) mixture of Li_2S_4, Li_2S_6, and Li_2S_8 in DOL/DME. Li atoms in violet, S atoms in yellow, DME molecules in red and DOL molecules in cyan. e) Cluster size distributions averaged over Li_2S_y (y=4, 6, and 8) DOL/DME classical MD simulations. Top: Li_2S_4. Middle: Li_2S_6. Bottom: Li_2S_8.

S2 and S3, respectively). Close Li-Li contacts are also rarer for the $(Li_2S_6)_z$ (z=1-6) and $(Li_2S_8)_z$ (z=1-3) clusters (see Table S2 and S3). In addition to greater amounts of aggregate sulfur, a higher Li:S ratio for the $(Li_2S_4)_z$ clusters may play a role in the greater number of close Li-Li contacts in the large $(Li_2S_4)_z$ clusters. As with the pure $(Li_2S_4)_z$ in DOL/DME solvent classical MD trajectory, larger $(Li_2S_6)_{z>4}$ clusters are observed (as shown in Figure 1e).

A comparison of the Li-Li PDF and NIPDF plots for $(Li_2S_4)_z$ (z=1-6), $(Li_2S_6)_z$ (z=1-4), and $(Li_2S_8)_z$ (z=1-3) from the classical MD simulations is shown in Figure S2. The PDFs indicate the presence of close-contact first-shell Li-Li interactions from about 2 to 3.1 Å (location of first peak) for the DOL/DME-solvated Li_2S_4 system which is in agreement with the presence of short Li-Li contacts observed in the large $(Li_2S_4)_6$ DFT-optimized cluster. Figure S2 also shows that the likelihood of short Li-Li contacts is much less likely for the DOL/DME-solvated $(Li_2S_6)_z$ (z=1-4), and $(Li_2S_8)_z$ (z=1-3) systems which is also in line with the limited number of lithium sulfide clusters we sampled from these systems. The trends in the number of close Li-Li distances for DOL/DME-solvated $(Li_2S_4)_z$ (z=1-6), $(Li_2S_6)_z$ (z=1-4), and $(Li_2S_8)_z$ (z=1-3) can be explained by the decreasing Li:S ratio going from $(Li_2S_4)_z$ (z=1-6) to $(Li_2S_8)_z$ (z=1-3). The decreasing Li:S ratio can also explain the decreasing Li-DOL oxygen and Li-DME oxygen contacts going from $(Li_2S_8)_z$ (z=1-3). The likelihood of Li accessible to the surface of the cluster decreases with lower overall content of Li in the cluster, reducing the Li-O solvent interactions at the interface of the cluster and solvent.

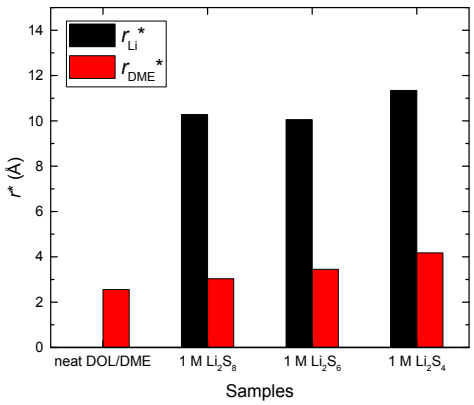

Figure 2. Effective hydrodynamic radius of Li^+ cations (r_{Li}*) and DME molecules (r_{DME}*) calculated using the Stokes-Einstein equation of diffusion from the measured diffusion coefficients D_{DOL}, D_{DME}, and D_{Li} at 30 °C.

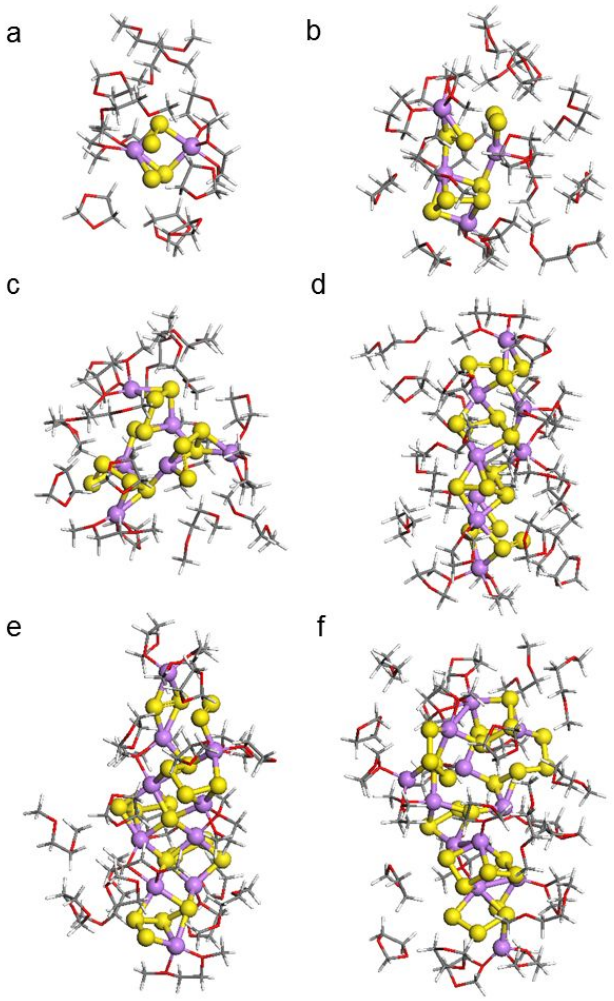

Figure 3. DFT-optimized clusters extracted from MD trajectory represented in Figure 1a. DOL/DME-solvated a) Li_2S_4, b) $(Li_2S_4)_2$, c) $(Li_2S_4)_3$, d) $(Li_2S_4)_4$, e) $(Li_2S_4)_5$, and f) $(Li_2S_4)_6$. Li atoms in violet, S atoms in yellow, C atoms in gray, H atoms in white, and O atoms in red.

4.2 Spectroscopic evidence for Li_xS_y clustering.

First, experimental NMR ^7Li, ^{17}O(DME), and ^{17}O(DOL) isotropic chemical shifts for the DOL/DME-solvated Li_2S_4,Li_2S_6, and Li_2S_8 systems are shown in Figure 6 and the DFT-calculated NMR isotropic chemical shifts based on the optimized clusters shown in Figures 3, 4, 5, and S3 are listed in Table 1. The experimental results shown in Figure 6 indicate that the DOL/DME-solvated Li_2S_4 system has the greatest ^7Li chemical shift value with respect to the Li^+ in water, followed by the chemical shift for the DOL/DME-solvated Li_2S_6 system, and, finally, the chemical shift for the Li_2S_8 system. With respect to ^{17}O in water, the greatest upfield (negative) shift for ^{17}O in DME occurs with the Li_2S_6 system, followed by the chemical shifts for the Li_2S_4 system, and, finally, the chemical shifts for the Li_2S_8 system. However, the change in chemical shifts with temperature with the DOL case is much less dramatic compared to the DME case. (Figure S4) The chemical shifts for DME and

DOL alone have been reported to be -23 to -23.9 ppm[65-67] and 33.5 to 34.8 ppm,[65, 68-70] respectively.

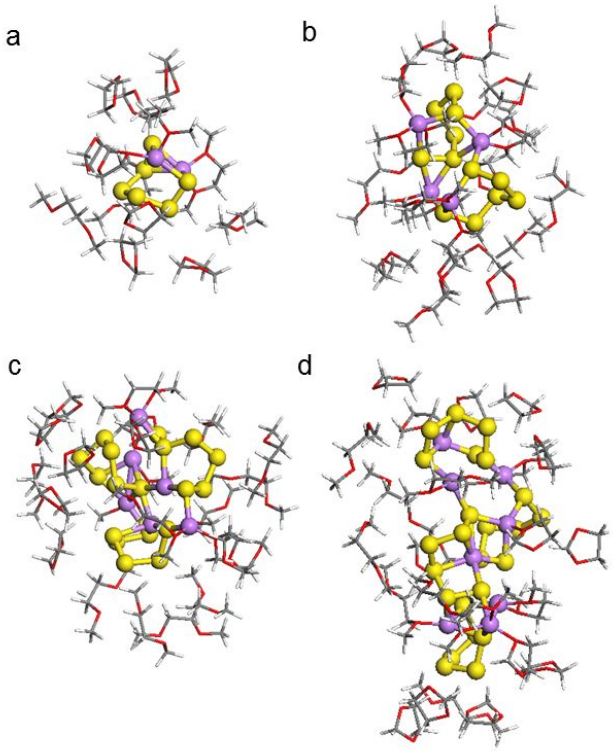

Figure 4. DFT-optimized clusters extracted from MD trajectory represented in Figure 1b. DOL/DME-solvated a) Li_2S_6, b) $(Li_2S_6)_2$, c) $(Li_2S_6)_3$, and d) $(Li_2S_6)_4$. Li atoms in violet, S atoms in yellow, C atoms in gray, H atoms in white, and O atoms in red.

Our measured chemical shifts for neat DME and DOL are in excellent agreement with the literature values (-24.2 and 34.7 ppm, respectively). Little change in the chemical shifts of DME and DOL are observed with a 1:1 volume mixture of DME and DOL (-24.8 and 34.7 ppm, respectively).

Comparing the experimental results with those from theory in Table 1, DFT-calculated ^{7}Li and ^{17}O chemical shifts are systematically slightly shifted to upfield (more negative ppm) and to downfield (more positive ppm), respectively, than the experimental shifts overall. The calculated ^{7}Li and ^{17}O chemical shifts based on an optimized cluster structure assume a temperature of 0 K which may account for these trends compared with experimental chemical shifts. The upfield shift of ^{7}Li resonances and downfield shift of ^{17}O resonances for DME molecules with decrease of temperature were confirmed experimentally from the ^{7}Li and ^{17}O NMR spectra, respectively, obtained at the temperature range of 293 – 333 K for the DOL/DME-solvated Li_2S_4, Li_2S_6, and Li_2S_8 systems (Figure S4). With increasing cluster size, the calculated ^{7}Li chemical shifts of the DOL/DME-solvated Li_2S_4 system show a downfield, increasingly positive trend in the chemical shift. For the Li_2S_6 and Li_2S_8 systems, we do not see a clear increasing or decreasing trend in the calculated ^{7}Li chemical shifts with increasing cluster size. With the limited sampling size of the cluster models, clear trends in ^{7}Li chemical shifts between the three different lithium sulfides cannot be readily discerned. The combined experimental and theoretical work of Wan et al. suggests that a dilute concentration of LiFSI salt fully dissociates to Li^+ and FSI^- in DME.[66] Therefore, they claim Li^+ would be totally solvated by DME molecules (bolstered by their MD and DFT simulations), and they assigned their dilute Li^+ chemical shift peak of -1.7 ppm to Li^+ surrounded by only DME molecules. We considered a number of Li^+-solvent configurations and calculated their ^{7}Li chemical shifts. These results are listed in Table S4. From the calculated chemical shifts for the $Li^+(DME)_2$ and $Li^+(DME)_3$ complexes in Table S4, we see that these values are -0.3 to -0.4 ppm more negative than the experimental -1.7 ppm chemical shift reported by Wan et al. for fully DME-solvated Li^+. This indicates that, if we shift our calculated ^{7}Li chemical shifts to positive by 0.3 to 0.4 ppm, they would be more comparable to our experimental ^{7}Li chemical shifts. This shift in our calculated results suggest that large $(Li_2S_4)_z$ clusters may be favored in the DOL/DME-solvated Li_2S_4 system rather than monomer Li_2S_4 and small $(Li_2S_4)_z$ clusters with $z \leq 6$. For the Li_2S_6 and Li_2S_8 systems, both monomeric and aggregate lithium sulfide cluster species may coexist. Li^+ fully solvated by only solvent molecules DME and/or DOL may not be favorable for any of the three lithium sulfide-DOL/DME solvent systems due to the experimental ^{7}Li chemical shifts being above 0 ppm.

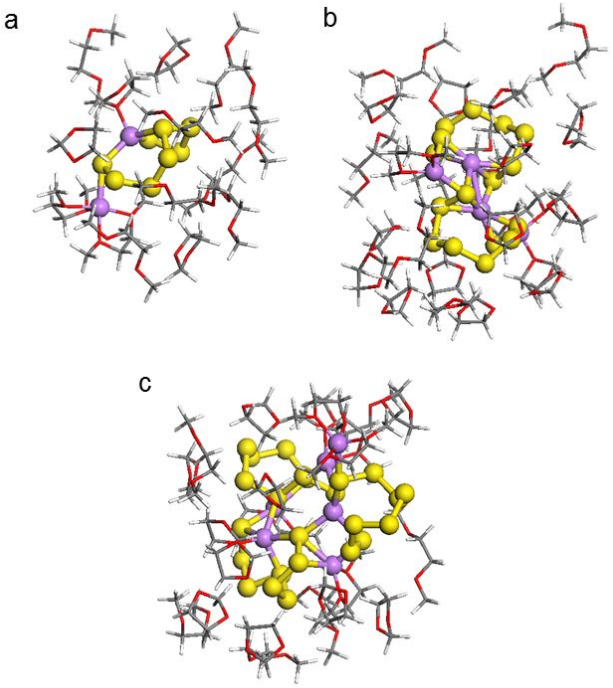

Figure 5. DFT-optimized clusters extracted from MD trajectory represented in Figure 1c. DOL/DME-solvated a) Li_2S_8, b) $(Li_2S_8)_2$, and c) $(Li_2S_8)_3$. Li atoms in violet, S atoms in yellow, C atoms in gray, H atoms in white, and O atoms in red.

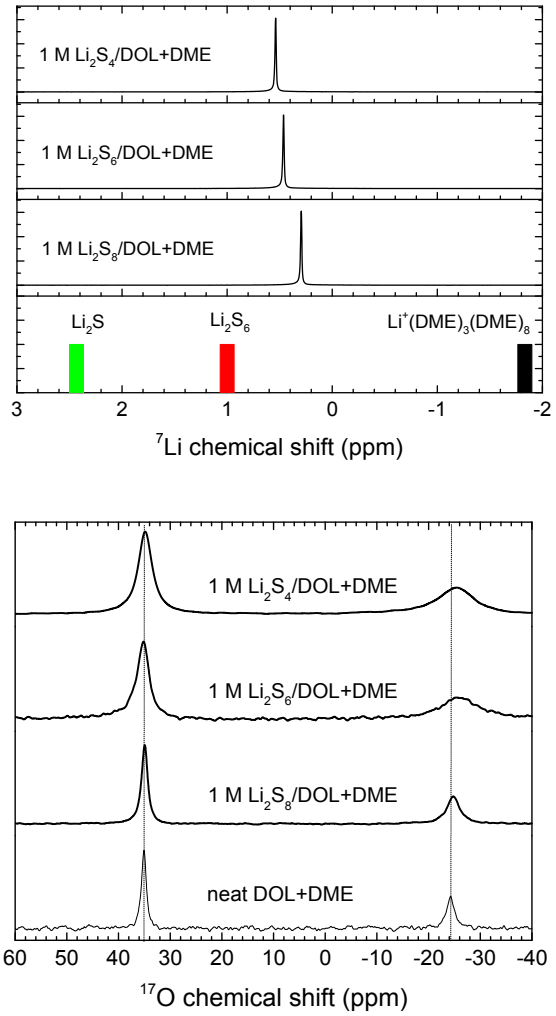

Figure 6. 7Li (top) and 17O (bottom) NMR spectra obtained from the DOL/DME-solvated Li2S4, Li2S6, and Li2S8 systems at 298 K. The 7Li chemical shifts of solid Li2S and Li2S6 are centered at 2.3 and 1.0 ppm, respectively and of Li2Sn (n = 2, 4 and 8) are the linear combinations of these two peaks.17 The Li^+ cation totally solvated by 11 DME molecules: $Li^+(DME)_3(DME)_8$ appears at -1.7 ppm.

For the calculated ^{17}O chemical shifts in Tables S4, we see an underestimation of the pure DME ^{17}O chemical shift by 5.7 ppm and the pure DOL ^{17}O chemical shift by 2.2 ppm. Improvements in the calculated ^{17}O chemical shifts can be realized with a larger 6-311++G(2d,2p) basis set[71, 72] (-20.3 ppm and 32.4 ppm for DME and DOL, respectively); however, this basis set size results in expensive chemical shift response calculations for the large lithium sulfide clusters.

Thus, we used the smaller 6-31G* basis set for all the systems as it represents the best compromise between computational efficiency and accuracy across the range of clusters considered in this study. According to the trend in Table S4, the complexation of DME and DOL with a single Li^+ cation results in a calculated upfield -5.4 to -2.8 ppm ^{17}O shift from pure DME and a calculated downfield 4.5 to 5.1 ppm ^{17}O shift from pure DOL. Table 1 shows a considerable variation in the ^{17}O shift for the calculated ^{17}O chemical shifts of DME for the DOL/DME-solvated lithium sulfide cluster systems around the calculated ^{17}O pure DME chemical shift. For the ^{17}O DOL chemical shift listed in Table 1, the calculated DOL ^{17}O chemical shifts of the DOL/DME-solvated lithium sulfide clusters shown an overall downfield shift; however, these values do not reach the extent of the magnitude of ^{17}O shifts shown for the calculated single Li^+ cation completely surrounded by only solvent molecules in Table S4. According to the experimental chemical shifts from the DOL/DME-solvent only baseline in Figure 6, the degree of downfield shift in ^{17}O NMR for the DOL in the DOL/DME-solvated lithium sulfide systems is slight, which is more indicative of the presence of mixed DOL/lithium sulfide clusters rather than full solvation of Li^+ by only the solvent molecules when comparing the Table 1 DOL/DME-solvated lithium sulfide cluster relative shifts to the larger relative shifts of Table S4 for the single Li^+ fully solvated by DME and/or DOL.

Table 1. DFT-calculated ^7Li and ^{17}O average isotropic chemical shifts for DFT-optimized DOL/DME-solvated Li_xS_y clusters extracted from Figure 1 MD trajectories (shown in Figures 3, 4, 5, and S3).

Li_xS_y cluster	ave. ^7Li δ_{iso} (ppm)	ave. DME ^{17}O δ_{iso} (ppm)	ave. DOL ^{17}O δ_{iso} (ppm)
$(Li_2S_4)_z$ species			
Li_2S_4	-2.4	-16.6	33.3
$(Li_2S_4)_2$	-1.8	-16.0	32.5
$(Li_2S_4)_3$	-1.4	-17.1	35.0
$(Li_2S_4)_4$	-1.2	-18.3	31.8
$(Li_2S_4)_5$	-1.6	-17.2	35.7
$(Li_2S_4)_6$	-0.7	-16.8	31.2
$(Li_2S_6)_z$ species			
Li_2S_6	-0.6	-15.2	32.4
$(Li_2S_6)_2$	0.0	-16.8	32.7
$(Li_2S_6)_3$	-0.2	-14.9	33.9
$(Li_2S_6)_4$	0.3	-15.5	34.1
$(Li_2S_8)_z$ species			
Li_2S_8	0.0	-18.5	35.4
$(Li_2S_8)_2$	-0.7	-15.2	35.2
$(Li_2S_8)_3$	0.2	-18.1	36.1
mixed species			
$(Li_2S_6)(Li_2S_8)$	0.2	-18.4	30.8
$(Li_2S_4)(Li_2S_6)_3$	-0.2	-16.0	31.3

Finally, the increase in the linewidths of both the DME and DOL peaks with decreasing sulfide chain from eight to four sulfur atoms can be explained by the variability in shared solvent/sulfide coordination. DME and DOL joint solvation of Li^+ with sulfide has the most variability in coordination scenarios for the DOL/DME-solvated Li_2S_4 system according to Table S1, especially for the larger clusters we considered in the DFT calculations. The DOL/DME-solvated Li_2S_6 clusters show a little less variety in joint solvent/sulfide chain coordination of Li^+ as compared to the Li_2S_4 clusters (see Table S2), and the DOL/DME-solvated Li_2S_8 show the least variability in joint solvent/sulfide chain Li^+ coordination (see Table S3). Thus, the spectral broadening Δ for the lithium sulfur clusters follow the trend $\Delta(Li_2S_8) < \Delta(Li_2S_6) < \Delta(Li_2S_4)$. The less broadened DOL peak in the lithium sulfide systems compared to the DME peak in these same systems can be explained by the observation that the DFT-optimized clusters show less joint complexation of the DOL with Li^+ compared to that of DME (see Tables S1, S2, and S3).

To further confirm the likely presence of lithium sulfide chain clustering in DOL/DME solvent, we performed S K-edge XAS measurements and, using cluster models shown in Figures 3-5), XANES simulations. Figure 7 shows a systematic comparison of simulated XANES plots based on model $(Li_2S_4)_z$ clusters, z=1-6 with experimentally-determined XANES of the DOL/DME-solvated Li_2S_4 system. The best agreement with the experimental S K-edge XANES spectrum for this system is shown by the simulated S K-edge XANES of the largest Li_2S_4 cluster, indicating that lithium sulfide chain aggregation may be likely for the DOL/DME-solvated Li_2S_4 system. The dashed and dash-dot vertical line indicate the peak centers of the terminal and internal sulfur atoms in the sulfide chains of the clusters, respectively. Spectral decomposition of the largest clusters considered for Li_2S_4, Li_2S_6, and Li_2S_8 into the terminal and internal S spectra are shown in Figure S5. This decomposition has been demonstrated in the work of Prendergast et al.[20] The experimental and simulated S K-edge XANES spectra comparison for the DOL/DME-solvated Li_2S_6 system is shown in Figure 8. The simulated XANES spectra of the larger $(Li_2S_6)_3$ and $(Li_2S_6)_4$ cluster models appear to best capture the features of the experimental XANES spectra, further bolstering the argument for lithium sulfur clustering in these systems.

Finally, Figure 9 compares the simulated and experimental S K-edge XANES spectra for the DOL/DME-solvated Li_2S_8 system. Again, as seen with the Li_2S_4 and Li_2S_6 systems, the best agreement spectrum with respect to the experimental XANES spectrum is the XANES spectrum generated from the largest DFT-optimized Li_2S_8 cluster considered in this study, $(Li_2S_8)_3$. Similar S K-edge XANES features are observed in DFT-optimized mixed sulfide chain clusters (Figure S6). These results further support the case for lithium sulfide aggregation in these electrolytes.

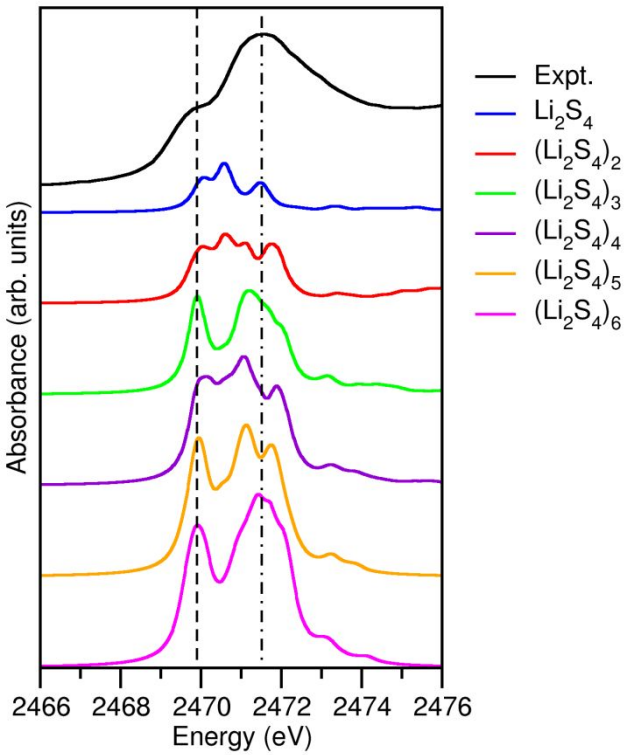

Figure 7. Sulfur K-edge XANES TDDFT calculations for the six complexes shown in (Li2S4)z (z=1-6) cluster Figures 3a-f compared with experiment. The simulated spectra have been Lorentzian-broadened by 0.5 eV and blue shifted by 52.5 eV.

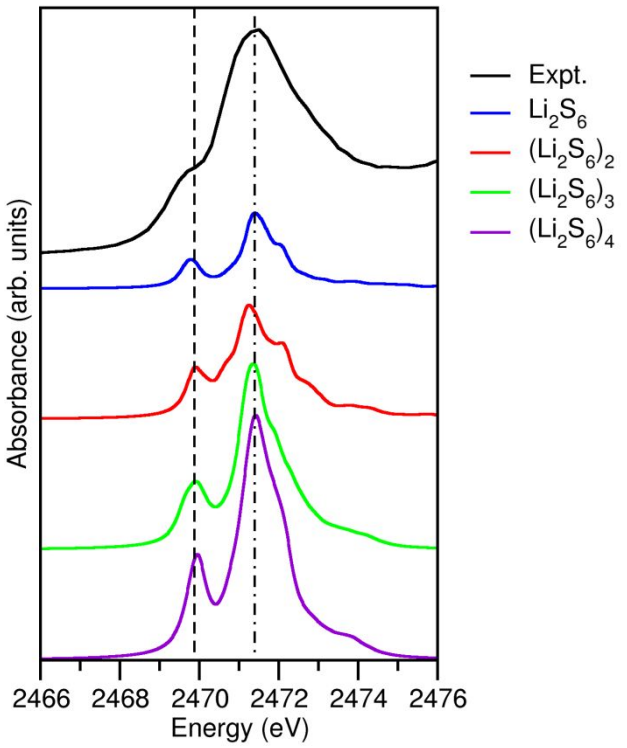

Figure 8. Sulfur K-edge XANES TDDFT calculations for the four complexes shown in $(Li_2S_6)_z$ (z=1-4) cluster Figures 3a-d compared with experiment. The simulated spectra have been Lorentzian-broadened by 0.5 eV and blue shifted by 52.5 eV.

4.3 Mobility and exchangeability of lithium.

To explore how readily Li^+ can dissociate from sulfide chains into the DOL/DME solvent, ab initio metadynamics simulations were performed on DOL/DME-solvated Li_2S_4, Li_2S_6, and Li_2S_8 monomers, tracking the free energy of a single Li^+ moving from the sulfide chain into DOL/DME solvent and from the solvent back to the sulfide chain. A low barrier to sulfide chain coordination to full DOL/DME oxygen coordination demonstrates facile mobility of Li^+ without the sulfide chain carrier and the likelihood of Li^+ exchange between sulfide chains and clusters.

As discussed previously, the lithium sulfide cluster size analysis from the conventional classical MD simulations suggests that single Li^+ cations, fully dissolved in DOL/DME, can be present in small amounts in the DOL/DME- solvated Li_2S_6 and Li_2S_8 (see Figure 1e) with single fully DOL/DME-solvated Li^+ cations being more likely in the Li2S8 system compared to the Li2S6 system. Recent conventional ab initio MD simulations of a single Li2S6 chain in DOL/DME solvent by Kamphaus and Balbuena14 suggest that Li^+ cations do not dissociate from the sulfur chains. However, the durations of Kamphaus and Balbuena's simulations were very short (15 ps) which may not have allowed enough time to elapse for a rare Li^+-sulfide chain dissociations to occur. With the enhanced metadynamics sampling method we find multiple free energy minima (Figure 10) for joint solvent oxygen-sulfide single Li^+ coordination for all three lithium sulfide systems. For the Li2S4 system, the dissociation free energy barrier of a single Li^+ into the solvent from the minimum at (1.14, 1.27) to the minimum at (0.15, 2.40) is 0.28 eV, and the free energy of reaction is 0.25 eV. For the Li2S6 system, the free energy barrier to a single Li^+ dissociation from the minimum at (1.61, 1.53) to the minimum at (0.14, 2.43) is 0.56 eV, and the free energy of reaction is -0.15 eV. Finally, for the Li2S8 system, the free energy barrier to a single Li^+ dissociation from the minimum at (0.95, 2.07) to the minimum at (0.26, 3.05) is to the Li^+ dissociation into the solvent minimum is in closer proximity in the Li2S4 system compared to that of the Li2S6 system. Though the Li^+ dissociation barrier and reaction free energy is more favorable in the Li2S4 system compared to that of the Li2S6 system, the lowest energy minimum in the Li2S4 system, 0.15 eV lower than the minimum before Li^+ dissociation, is at (2.72, 0.19), and the Li2S6 system Li^+ dissociation reaction free energy is exothermic with the full Li^+ solvation by DOL/DME minimum being the lowest energy minimum. Thus, Li^+ dissociation in the Li2S6 system may be more favorable than that for the Li2S4 system. Li^+ dissociation in the Li2S8 system may be more favorable than either the Li2S4 and Li2S6 due to the closer proximity of the Li^+ S, O-coordination space minimum for joint sulfur/oxygen coordination compared to that of Li2S4 and Li2S6 systems and to the lower free energy barrier to Li^+ dissociation compared to that of the Li2S6 system (despite the minimum for full Li^+ DOL/DME solvation being the lowest minimum for the Li2S6 system). Similar observations have been reported in previous work.[10, 13]

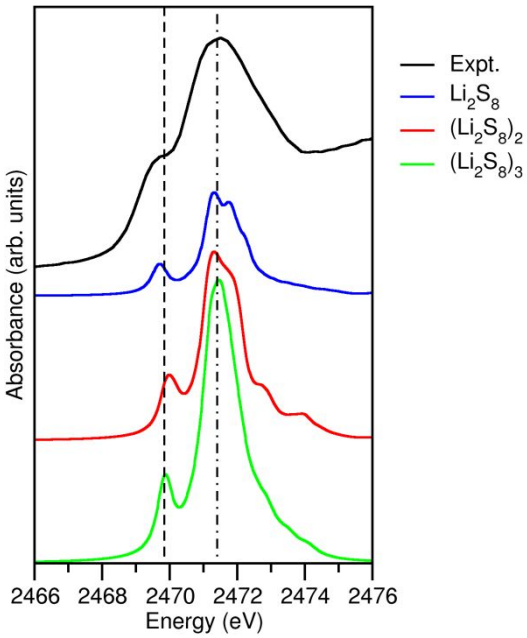

Figure 9. Sulfur K-edge XANES TDDFT calculations for the three complexes shown in $(Li_2S_8)_z$ (z=1-3) cluster Figures 4a-c compared with experiment. The simulated spectra have been Lorentzian-broadened by 0.5 eV and blue shifted by 52.5 eV.

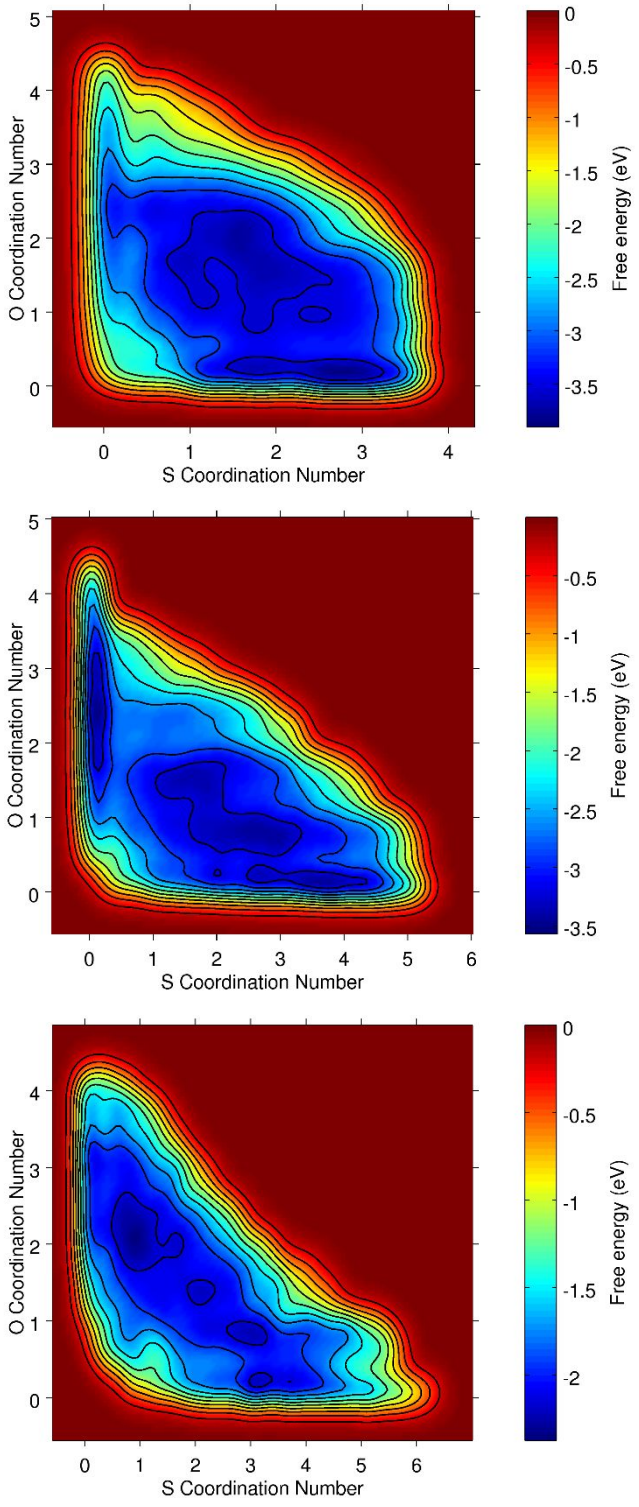

Figure 10. Free energy surface contour plots for S_x cluster sulfur coordination number versus solvent oxygen coordination number for one lithium atom from metadynamics simulations. Top: Li_2S_4. Middle: Li_2S_6. Bottom: Li_2S_8.

We note that the Li^+ mobility mechanism explored here: e.g., between sulfide chains and clusters of sulfide chains to/from the DOL/DME solvent is likely not the only available pathway. In addition, interchain/intercluster Li^+ exchange can occur through the dynamics of sulfide chain/sulfide chain cluster aggregation and dissolution which are observed to occur continuously throughout the classical MD simulations. The diffusion measurements from PFG-NMR (Figure S8) indicate that, with consistently slower diffusion relative to that of both DME and DOL in all three lithium sulfide systems considered here ($D(Li_2S_4)<D(Li_2S_6)<D(Li_2S_8)$), Li^+ is likely shuttled by heavier sulfide chains and clusters of sulfide chains. Therefore, the major mechanism of Li^+ exchange and diffusion is likely Li^+ shuttling by sulfide chains/sulfide chain clusters, and Li^+ exchange and diffusion through Li^+-sulfide chain/cluster dissociation to the DOL/DME solvent is a minor mechanism. This observation is supported by experimental and theoretical NMR, classical conventional MD and ab initio metadynamics simulations.

5. CONCLUSIONS

We have performed NMR and XAS experiments, computational NMR and XANES spectroscopy calculations, classical conventional MD and ab initio metadynamics simulations to unravel the lithium polysulfide clustering and associated dynamic processes. In particular, the Li^+ mobility, and inter-sulfide chain/cluster Li^+ exchange processes under varying polysulfide chain lengths (i.e., Li_2S_4, Li_2S_6, and Li_2S_8 systems) solvated by a 1:1 DOL/DME solvent mixture were studied. From the classical MD simulations of a complex mixtures of 1 M Li_2S_4, Li_2S_6, or Li_2S_8 in a 1:1 DOL/DME solvent, we show aggregation of lithium sulfide chains for these three sulfide systems resulting in varying distributions of lithium sulfide chain cluster size. The classical MD simulations and DFT-optimized clusters demonstrate joint Li^+ coordination by the DOL/DME solvent molecules and sulfide chains. A detailed analysis of the Li^+ coordination in each of the cluster models uncovers a progressive decrease in the participation of DME and DOL oxygen atoms in the joint coordination of Li^+ with the sulfide sulfur atoms from Li_2S_4 to Li_2S_8. Compared to the DOL involvement in joint Li^+ coordination, the DME shows the most variation in modes of Li^+ joint coordination and the greatest involvement in Li^+ joint coordination. The analysis of the experimental and calculated ^7Li and ^{17}O NMR chemical shifts and PFG-NMR diffusion measurements corroborate the direct structural findings from our classical MD and DFT simulations. From the simulated S K-edge XANES spectra of various polysulfide clusters, we demonstrate that higher order cluster size in all three DOL/DME-solvated lithium sulfide systems shows better agreement with experimental spectra.

These polysulfide clustering process has profound implications in electrochemical performance of Li-S battery. For example, during the discharge process the

cleavage of sulfur rings by incoming lithium cations would lead to localized high concentration of lithium polysulfide species at the cathode-electrolyte interface. Due to higher solubility of initial polysulfide species (mostly long chain Li_2S_n, $4<n\leq8$), it is very likely to have polysulfide clusters identified in this work, as major constituents at the interface regime and subsequently the initiating event of shuttling process towards Li-metal anode. In addition, during the charging process these polysulfide clusters will engage in nucleation process supported by sulfur ring recombination. This nucleation will determine sulfur redistribution and ultimately the cathode integrity. The atomistic view of polysulfide clustering process will help design the carbon substrate that can help us control the morphology and redistribution and ultimately achieve maximum utilization of sulfur.

Finally, we demonstrate from our analyses of classical conventional MD and ab initio metadynamics simulations and experimental and calculated NMR results that solvent solvation of Li^+ (e.g., only the DOL/DME solvent molecules) following Li^+ dissociation from sulfide chains/clusters is plausible. The emergence of "free" Li^+, however, is likely a minor contributor to interchain/cluster Li^+ exchange. The major contributor to interchain/cluster Li^+ exchange is likely the dynamic processes of sulfide chain/cluster aggregation and dissolution that shuttle Li^+ from one chain/cluster to another. These fundamental details of lithium exchange dynamics between solvent and polysulfide species, can help us in electrolyte design and provide greater control of the solvated lithium polysulfide cluster generation process. Overall, both polysulfide clustering process and lithium exchange dynamics will help us gain predictive understanding of lithium-sulfur electrochemical process.

ASSOCIATED CONTENT

Supporting Information. PDF and NIPDF plots, coordination of each lithium atom for each of the $(Li_2S_4)_z$(z=1-6), $(Li_2S_6)_z$ (z=1-4) and $(Li_2S_8)_z$ (z=1-3), tables for atom coordination numbers in DFT-optimized lithium sulfide cluster structures, the DFT-optimized structure of mixed lithium sulfide clusters, selected decomposed simulated XANES spectra for the $(Li_2S_4)_z$(z=1-6), $(Li_2S_6)_z$ (z=1-4) and $(Li_2S_8)_z$ (z=1-3) systems, simulated XANES spectra for mixed lithium sulfide clusters, DFT-calculated ^{17}O and ^{7}Li chemical shifts for small Li^+-DOL/DME clusters, and temperature dependent experimental PFG-NMR diffusion plot. This material is available free of charge via the Internet at http://pubs.acs.org.

AUTHOR INFORMATION

Corresponding Authors

* (V.M.) E-mail: vijay@pnnl.gov.
* (A.A.) E-mail: amity.andersen@pnnl.gov.

ORCID

Amity Andersen: 0000-0002-6529-0905
Nav Nidhi Rajput: 0000-0003-4740-8217
Kee Sung Han: 0000-0002-3535-1818
Huilin Pan 0000-0001-7991-1015
Niranjan Govind: 0000-0003-3625-366X
Kristin A. Persson: 0000-0003-2495-5509
Karl T. Mueller: 0000-0001-9609-9516
Vijayakumar Murugesan: 0000-0001-6149-1702

Present Address

†Chemical and Biological Engineering, Tufts University, Science and Technology Center, 4 Colby Street, Medford, Massachusetts, 02155, United States. E-mail: navnidhi.rajput@tufts.edu.

ACKNOWLEDGMENT

This research was intellectually led by the Joint Center for Energy Storage Research (JCESR), an Energy Innovation Hub funded by the U.S. Department of Energy (DOE), Office of Science, Basic Energy Sciences (BES), under Contract No. DEAC02-06CH11357. Computational studies and NMR experiments were performed at the Environmental Molecular Sciences Laboratory (EMSL), a DOE Office of Science User Facility sponsored by the Office of Biological and Environmental Research and located at Pacific Northwest National Laboratory. Additionally, the research used resources of the National Energy Research Scientific Computing Center, a DOE Office of Science User Facility supported by the Office of Science of the DOE under contract no. DE-AC02-05CH1123.

REFERENCES

1. Zhang, S. S., Liquid electrolyte lithium/sulfur battery: Fundamental chemistry, problems, and solutions. *J. Power Sources* **2013,** 231, 153-162.
2. Manthiram, A.; Fu, Y.; Su, Y.-S., Challenges and Prospects of Lithium–Sulfur Batteries. *Acc. Chem. Res.* **2013,** 46, 1125-1134.
3. Bruce, P. G.; Freunberger, S. A.; Hardwick, L. J.; Tarascon, J.-M., Li–O2 and Li–S batteries with high energy storage. *Nature Mater.* **2011,** 11, 19.
4. Manthiram, A.; Fu, Y.; Chung, S.-H.; Zu, C.; Su, Y.-S., Rechargeable Lithium–Sulfur Batteries. *Chem. Rev.* **2014,** 114, 11751-11787.
5. Shin, E. S.; Kim, K.; Oh, S. H.; Cho, W. I., Polysulfide dissolution control: the common ion effect. *Chem. Commun.* **2013,** 49, 2004-2006.
6. Chen, J.; Han, K. S.; Henderson, W. A.; Lau, K. C.; Vijayakumar, M.; Dzwiniel, T.; Pan, H.; Curtiss, L. A.; Xiao, J.; Mueller, K. T.; Shao, Y.; Liu, J., Restricting the Solubility of Polysulfides in Li-S Batteries Via Electrolyte Salt Selection. *Adv. Energy Mater.* **2016,** 6, 1600160.
7. Diao, Y.; Xie, K.; Xiong, S.; Hong, X., Shuttle phenomenon – The irreversible oxidation mechanism of sulfur active material in Li–S battery. *J. Power Sources* **2013,** 235, 181-186.
8. Marmorstein, D.; Yu, T. H.; Striebel, K. A.; McLarnon, F. R.; Hou, J.; Cairns, E. J., Electrochemical

performance of lithium/sulfur cells with three different polymer electrolytes. *J. Power Sources* **2000,** 89, 219-226.
9. Tobishima, S.; Morimoto, H.; Aoki, M.; Saito, Y.; Inose, T.; Fukumoto, T.; Kuryu, T., Glyme-based nonaqueous electrolytes for rechargeable lithium cells. *Electrochim. Acta* **2004,** 49, 979-987.
10. Vijayakumar, M.; Govind, N.; Walter, E.; Burton, S. D.; Shukla, A.; Devaraj, A.; Xiao, J.; Liu, J.; Wang, C.; Karim, A., Molecular structure and stability of dissolved lithium polysulfide species. *Phys. Chem. Chem. Phys.* **2014,** 16, 10923-10932.
11. Wang, L.; Zhang, T.; Yang, S.; Cheng, F.; Liang, J.; Chen, J., A quantum-chemical study on the discharge reaction mechanism of lithium-sulfur batteries. *J. Energy Chem.* **2013,** 22, 72-77.
12. Han, K. S.; Chen, J.; Cao, R.; Rajput, N. N.; Murugesan, V.; Shi, L.; Pan, H.; Zhang, J.-G.; Liu, J.; Persson, K. A.; Mueller, K. T., Effects of Anion Mobility on Electrochemical Behaviors of Lithium–Sulfur Batteries. *Chem. Mater.* **2017,** 29, 9023-9029.
13. Rajput, N. N.; Murugesan, V.; Shin, Y.; Han, K. S.; Lau, K. C.; Chen, J.; Liu, J.; Curtiss, L. A.; Mueller, K. T.; Persson, K. A., Elucidating the Solvation Structure and Dynamics of Lithium Polysulfides Resulting from Competitive Salt and Solvent Interactions. *Chem. Mater.* **2017,** 29, 3375-3379.
14. Kamphaus, E. P.; Balbuena, P. B., First-Principles Investigation of Lithium Polysulfide Structure and Behavior in Solution. *J. Phys. Chem. C* **2017,** 121, 21105-21117.
15. Najmus, S.; Cody, J. S.; Maupin, C. M.; Jason, M. P., A Novel Optical Diagnostic for In Situ Measurements of Lithium Polysulfides in Battery Electrolytes. *Appl. Spectrosc.* **2017,** 71, 1593-1599.
16. Barchasz, C.; Molton, F.; Duboc, C.; Leprêtre, J.-C.; Patoux, S.; Alloin, F., Lithium/Sulfur Cell Discharge Mechanism: An Original Approach for Intermediate Species Identification. *Anal. Chem.* **2012,** 84, 3973-3980.
17. Cuisinier, M.; Cabelguen, P.-E.; Evers, S.; He, G.; Kolbeck, M.; Garsuch, A.; Bolin, T.; Balasubramanian, M.; Nazar, L. F., Sulfur Speciation in Li–S Batteries Determined by Operando X-ray Absorption Spectroscopy. *J. Phys. Chem. Lett.* **2013,** 4, 3227-3232.
18. Hannauer, J.; Scheers, J.; Fullenwarth, J.; Fraisse, B.; Stievano, L.; Johansson, P., The Quest for Polysulfides in Lithium–Sulfur Battery Electrolytes: An Operando Confocal Raman Spectroscopy Study. *ChemPhysChem* **2015,** 16, 2755-2759.
19. Cuisinier, M.; Hart, C.; Balasubramanian, M.; Garsuch, A.; Nazar, L. F., Radical or Not Radical: Revisiting Lithium–Sulfur Electrochemistry in Nonaqueous Electrolytes. *Adv. Energy Mater.* **2015,** 5, 1401801.
20. Pascal, T. A.; Wujcik, K. H.; Velasco-Velez, J.; Wu, C.; Teran, A. A.; Kapilashrami, M.; Cabana, J.; Guo, J.; Salmeron, M.; Balsara, N.; Prendergast, D., X-ray Absorption Spectra of Dissolved Polysulfides in Lithium–Sulfur Batteries from First-Principles. *J. Phys. Chem. Lett.* **2014,** 5, 1547-1551.
21. Wujcik, K. H.; Velasco-Velez, J.; Wu, C. H.; Pascal, T.; Teran, A. A.; Marcus, M. A.; Cabana, J.; Guo, J.; Prendergast, D.; Salmeron, M.; Balsara, N. P., Fingerprinting Lithium-Sulfur Battery Reaction Products by X-ray Absorption Spectroscopy. *J. Electrochem. Soc.* **2014,** 161, A1100-A1106.
22. Hagen, M.; Schiffels, P.; Hammer, M.; Dörfler, S.; Tübke, J.; Hoffmann, M. J.; Althues, H.; Kaskel, S., In-Situ Raman Investigation of Polysulfide Formation in Li-S Cells. *J. Electrochem. Soc.* **2013,** 160, A1205-A1214.
23. Wang, Q.; Zheng, J.; Walter, E.; Pan, H.; Lv, D.; Zuo, P.; Chen, H.; Deng, Z. D.; Liaw, B. Y.; Yu, X.; Yang, X.; Zhang, J.-G.; Liu, J.; Xiao, J., Direct Observation of Sulfur Radicals as Reaction Media in Lithium Sulfur Batteries. *J. Electrochem. Soc.* **2015,** 162, A474-A478.
24. Pascal, T. A.; Pemmaraju, C. D.; Prendergast, D., X-ray spectroscopy as a probe for lithium polysulfide radicals. *Phys. Chem. Chem. Phys.* **2015,** 17, 7743-7753.
25. Gorlin, Y.; Siebel, A.; Piana, M.; Huthwelker, T.; Jha, H.; Monsch, G.; Kraus, F.; Gasteiger, H. A.; Tromp, M., Operando Characterization of Intermediates Produced in a Lithium-Sulfur Battery. *J. Electrochem. Soc.* **2015,** 162, A1146-A1155.
26. Nandasiri, M. I.; Camacho-Forero, L. E.; Schwarz, A. M.; Shutthanandan, V.; Thevuthasan, S.; Balbuena, P. B.; Mueller, K. T.; Murugesan, V., In Situ Chemical Imaging of Solid-Electrolyte Interphase Layer Evolution in Li–S Batteries. *Chem. Mater.* **2017,** 29, 4728-4737.
27. Xiao, J.; Hu, J. Z.; Chen, H.; Vijayakumar, M.; Zheng, J.; Pan, H.; Walter, E. D.; Hu, M.; Deng, X.; Feng, J.; Liaw, B. Y.; Gu, M.; Deng, Z. D.; Lu, D.; Xu, S.; Wang, C.; Liu, J., Following the Transient Reactions in Lithium–Sulfur Batteries Using an In Situ Nuclear Magnetic Resonance Technique. *Nano Lett.* **2015,** 15, 3309-3316.
28. M. J. Abraham, D. v. d. S., E. Lindahl, B. Hess and the GROMACS development team, GROMACS User Manual version 5.1.2. **2016,** GROMACS User Manual version 5.1.2 www.gromacs.org.
29. Martínez, L.; Andrade, R.; Birgin, E. G.; Martínez, J. M., Packmol: A package for building initial configurations for molecular dynamics simulations. *J. Comput. chem.* **2009,** 30, 2157-2164.
30. Berendsen, H. J.; Postma, J. P. M.; van Gunsteren, W. F.; DiNola, A.; Haak, J., Molecular dynamics with coupling to an external bath. *J. Chem. Phys.* **1984,** 81, 3684-3690.

31. Bussi, G.; Donadio, D.; Parrinello, M., Canonical sampling through velocity rescaling. *J. Chem. Phys.* **2007,** 126, 014101.
32. Bussi, G.; Zykova-Timan, T.; Parrinello, M., Isothermal-isobaric molecular dynamics using stochastic velocity rescaling. *J. Chem. Phys.* **2009,** 130, 074101-9.
33. Humphrey, W.; Dalke, A.; Schulten, K., VMD: Visual molecular dynamics. *J. Mol. Graphics* **1996,** 14, 33-38 (http://www.ks.uiuc.edu/Research/vmd/).
34. Valiev, M.; Bylaska, E. J.; Govind, N.; Kowalski, K.; Straatsma, T. P.; Van Dam, H. J. J.; Wang, D.; Nieplocha, J.; Apra, E.; Windus, T. L.; de Jong, W. A., NWChem: A comprehensive and scalable open-source solution for large scale molecular simulations. *Comput. Phys. Commun.* **2010,** 181, 1477-1489.
35. Perdew, J. P.; Ernzerhof, M.; Burke, K., Rationale for mixing exact exchange with density functional approximations. *J. Chem. Phys.* **1996,** 105, 9982-9985.
36. Adamo, C.; Barone, V., Toward reliable density functional methods without adjustable parameters: The PBE0 model. *J. Chem. Phys.* **1999,** 110, 6158-6170.
37. Hariharan, P. C.; Pople, J. A., The influence of polarization functions on molecular orbital hydrogenation energies. *Theoret. Chim. Acta* **1973,** 28, 213-222.
38. Francl, M. M.; Pietro, W. J.; Hehre, W. J.; Binkley, J. S.; Gordon, M. S.; DeFrees, D. J.; Pople, J. A., Self-consistent molecular orbital methods. XXIII. A polarization-type basis set for second-row elements. *J. Chem. Phys.* **1982,** 77, 3654-3665.
39. Grimme, S., Semiempirical GGA-type density functional constructed with a long-range dispersion correction. *J. Comput. Chem.* **2006,** 27, 1787-1799.
40. Igel-Mann, G.; Stoll, H.; Preuss, H., Pseudopotentials for main group elements (IIIa through VIIa). *Mol. Phys.* **1988,** 65, 1321-1328.
41. *CP2K version 4.1, the CP2K developers group, CP2K is freely available from https://www.cp2k.org/*, 2016.
42. Hutter, J.; Iannuzzi, M.; Schiffmann, F.; VandeVondele, J., cp2k: atomistic simulations of condensed matter systems. *Wiley Interdisciplinary Reviews: Computational Molecular Science* **2014,** 4, 15-25.
43. VandeVondele, J.; Hutter, J., Gaussian basis sets for accurate calculations on molecular systems in gas and condensed phases. *J. Chem. Phys.* **2007,** 127, 114105.
44. Goedecker, S.; Teter, M.; Hutter, J., Separable dual-space Gaussian pseudopotentials. *Phys. Rev. B* **1996,** 54, 1703-1710.
45. Hartwigsen, C.; Goedecker, S.; Hutter, J., Relativistic separable dual-space Gaussian pseudopotentials from H to Rn. *Phys. Rev. B* **1998,** 58, 3641-3662.
46. Krack, M., Pseudopotentials for H to Kr optimized for gradient-corrected exchange-correlation functionals. *Theoret. Chem. Acc.* **2005,** 114, 145-152.
47. Vydrov, O. A.; Van Voorhis, T., Nonlocal van der Waals density functional: The simpler the better. *J. Chem. Phys.***2010,** 133, 244103.
48. Román-Pérez, G.; Soler, J. M., Efficient Implementation of a van der Waals Density Functional: Application to Double-Wall Carbon Nanotubes. *Phys. Rev. Lett.* **2009,** 103, 096102.
49. Sabatini, R.; Gorni, T.; de Gironcoli, S., Nonlocal van der Waals density functional made simple and efficient. *Phys. Rev. B* **2013,** 87, 041108.
50. Klamt, A.; Schuurmann, G., COSMO: a new approach to dielectric screening in solvents with explicit expressions for the screening energy and its gradient. *Journal of the Chemical Society, Perkin Transactions 2* **1993**, (5), 799-805.
51. Dyer, J. C.; Harris, D. L.; Evans, J., S. A, Oxygen-17 nuclear magnetic resonance spectroscopy of sulfoxides and sulfones. Alkyl substituent induced chemical shift effects. *J. Org. Chem.* **1982,** 47, 3660-3664.
52. Stener, M.; Fronzoni, G.; de Simone, M., Time dependent density functional theory of core electrons excitations. *Chemical Physics Letters* **2003,** 373, (1), 115-123.
53. Besley, N. A.; Noble, A., Time-Dependent Density Functional Theory Study of the X-ray Absorption Spectroscopy of Acetylene, Ethylene, and Benzene on Si(100). *The Journal of Physical Chemistry C* **2007,** 111, (8), 3333-3340.
54. DeBeer George, S.; Petrenko, T.; Neese, F., Time-dependent density functional calculations of ligand K-edge X-ray absorption spectra. *Inorg. Chim. Acta* **2008,** 361, (4), 965-972.
55. Liang, W.; Fischer, S. A.; Frisch, M. J.; Li, X., Energy-Specific Linear Response TDHF/TDDFT for Calculating High-Energy Excited States. *J. Chem. Theor. Comput.* **2011,** 7, 3540-3547.
56. Lopata, K.; Van Kuiken, B. E.; Khalil, M.; Govind, N., Linear-Response and Real-Time Time-Dependent Density Functional Theory Studies of Core-Level Near-Edge X-Ray Absorption. *J. Chem. Theor. Comput.* **2012,** 8, 3284-3292.
57. Van Kuiken, B. E.; Valiev, M.; Daifuku, S. L.; Bannan, C.; Strader, M. L.; Cho, H.; Huse, N.; Schoenlein, R. W.; Govind, N.; Khalil, M., Simulating Ru L3-Edge X-ray Absorption Spectroscopy with Time-Dependent Density Functional Theory: Model Complexes and Electron Localization in Mixed-Valence Metal Dimers. *The J. Phys. Chem. A* **2013,** 117, 4444-4454.
58. Zhang, Y.; Biggs, J. D.; Healion, D.; Govind, N.; Mukamel, S., Core and valence excitations in resonant

X-ray spectroscopy using restricted excitation window time-dependent density functional theory. *J. Chem. Phys.* **2012,** 137, 194306.
59. Vjunov, A.; Fulton, J. L.; Huthwelker, T.; Pin, S.; Mei, D.; Schenter, G. K.; Govind, N.; Camaioni, D. M.; Hu, J. Z.; Lercher, J. A., Quantitatively Probing the Al Distribution in Zeolites. *J. Am. Chem. Soc.* **2014,** 136, 8296-8306.
60. Fulton, J. L.; Govind, N.; Huthwelker, T.; Bylaska, E. J.; Vjunov, A.; Pin, S.; Smurthwaite, T. D., Electronic and Chemical State of Aluminum from the Single- (K) and Double-Electron Excitation (KLII&III, KLI) X-ray Absorption Near-Edge Spectra of α-Alumina, Sodium Aluminate, Aqueous Al3+·(H2O)6, and Aqueous Al(OH)4−. *J. Phys. Chem. B* **2015,** 119, 8380-8388.
61. Govind, N.; de Jong, W. A., Simulating Cl K-edge X-ray absorption spectroscopy in MCl6 2− (M = U, Np, Pu) complexes and UOCl5 − using time-dependent density functional theory. *Theoret. Chem. Acc.* **2014,** 133, 1463.
62. Ross, M. R.; Andersen, A.; Fox, Z. W.; Zhang, Y.; Hong, K.; Lee, J.-H.; Cordones, A. A.; March, A. M.; Doumy, G.; Southworth, S. H.; Marcus, M. A.; Schoenlein, R. W.; Mukamel, S.; Govind, N.; Khalil, M., A Comprehensive Experimental and Computational Spectroscopic Study of Hexacyanoferrate Complexes in Water: from the Infrared to X-ray Wavelengths. *The J. Phys. Chem. B* **2018**, 122, 5075-5086.
63. Ryckaert, J.-P.; Ciccotti, G.; Berendsen, H. J. C., Numerical integration of the cartesian equations of motion of a system with constraints: molecular dynamics of n-alkanes. *J. Comput. Phys.* **1977,** 23, 327-341.
64. Lee, J. H.; Han, K. S.; Lee, J. S.; Lee, A. S.; Park, S. K.; Hong, S. Y.; Lee, J.-C.; Mueller, K. T.; Hong, S. M.; Koo, C. M., Facilitated Ion Transport in Smectic Ordered Ionic Liquid Crystals. *Adv. Mater.* **2016,** 28, 9301-9307.
65. Sugawara, T.; Kawada, Y.; Katoh, M.; Iwamura, H., Oxygen-17 Nuclear Magnetic Resonance. III. Oxygen Atoms with a Coordination Number of Two. *Bull. Chem. Soc. Jpn.* **1979,** 52, 3391-3396.
66. Wan, C.; Hu, M. Y.; Borodin, O.; Qian, J.; Qin, Z.; Zhang, J.-G.; Hu, J. Z., Natural abundance 17O, 6Li NMR and molecular modeling studies of the solvation structures of lithium bis(fluorosulfonyl)imide/1,2-dimethoxyethane liquid electrolytes. *J. Power Sources* **2016,** 307, 231-243.
67. Peng, J.; Carbone, L.; Gobet, M.; Hassoun, J.; Devany, M.; Greenbaum, S., Natural Abundance Oxygen-17 NMR Investigation of Lithium Ion Solvation in Glyme-based Electrolytes. *Electrochim. Acta* **2016,** 213, 606-612.
68. Pihlaja, K.; Nummelin, H.; Klika Karel, D.; Czombos, J., 1H, 13C and 17O NMR spectral studies on monocyclic dioxolanes, dioxanes, dioxepanes and dioxocanes and cycloalkane-fused (5–8-membered) bicyclic 1,3-dioxolanes and 1,3-dioxanes. *Magn. Resonan. Chem.* **2001,** 39, 657-671.
69. Eliel, E. L.; Pietrusiewicz, K. M.; Jewell, L. M., O-17 NMR spectra of ring compounds. Correlation of 17O and 13C methyl substitution parameters. *Tetrahedron Lett.* **1979,** 20, 3649-3652.
70. Kintzinger, J.-P.; Delseth, C.; nguyên, T. T.-t., 17O nuclear magnetic resonance:mutual effect between two β oxygen atoms and α,β double bond effect on 17O chemical shift. *Tetrahedron* **1980,** 36, (23), 3431-3435.
71. Krishnan, R.; Binkley, J. S.; Seeger, R.; Pople, J. A., Self-consistent molecular orbital methods. XX. A basis set for correlated wave functions. *J. Chem. Phys.* **1980,** 72, 650-654.
72. McLean, A. D.; Chandler, G. S., Contracted Gaussian basis sets for molecular calculations. I. Second row atoms, Z=11–18. *J. Chem. Phys.* **1980,** 72, 5639-5648.

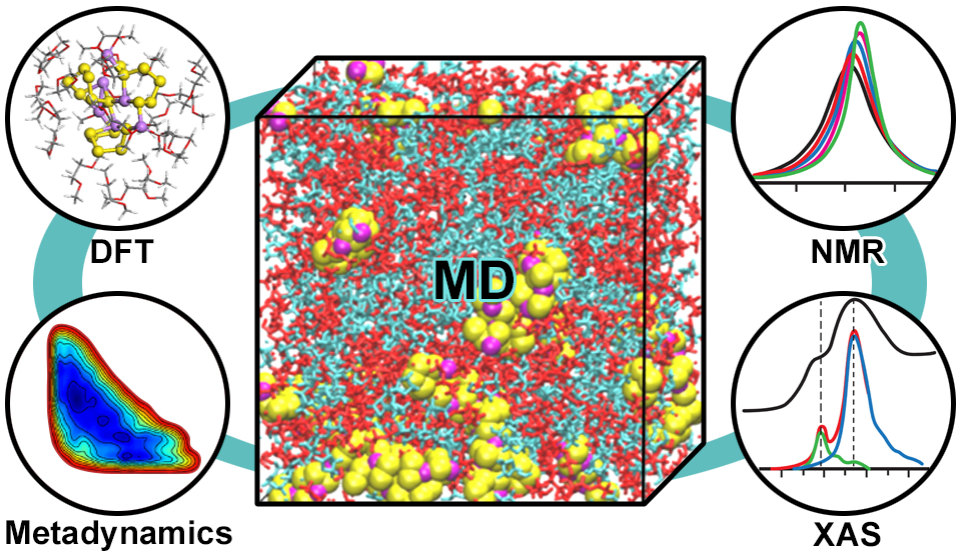

TOC graphics